

Research Paper

Characterization of Low-Velocity Impact Damage in Asymmetric Composite Shells

Luis Miguel Ferreira^{1,2}, Carlos A.C.P. Coelho³, Paulo N.B. Reis⁴

¹ Grupo de Elasticidad y Resistencia de Materiales, Escuela Técnica Superior de Ingeniería, Universidad de Sevilla, Camino Descubrimientos, S/N 41092 Sevilla, España, Email: lmarques@us.es

² Escuela Politécnica Superior, Universidad de Sevilla, C/ Virgen de África, 7, Sevilla, 41011, España

³ Unidade Departamental de Engenharias, Escola Superior de Tecnologia de Abrantes, Instituto Politécnico de Tomar, Rua 17 de Agosto de 1808 S/N 2200-370 Abrantes, Portugal, Email: cccampos@ipt.pt

⁴ University of Coimbra, CEMMPRE, ARISE, Department of Mechanical Engineering, 3030-780 Coimbra, Portugal, Email: paulo.reis@dem.uc.pt

Received January 29 2024; Revised April 21 2024; Accepted for publication June 04 2024.

Corresponding author: L.M. Ferreira (lmarques@us.es)

© 2024 Published by Shahid Chamran University of Ahvaz

Abstract. Based on numerical modelling, this study investigates asymmetric semicylindrical composite laminate shells' damage characteristics under low-velocity impact loads. For this purpose, several asymmetric stacking sequences were subjected to low-velocity impact and the results were analysed in terms of force, displacement, contact time, and absorbed energy. It is concluded that the maximum impact force decreases with an increase in the number of layers oriented at 0°, particularly in the upper half of the laminate. The laminates with a 45° orientation in the upper layers present the lowest displacement values, whereas the laminates with the upper layers oriented at 0° exhibit longer contact times. It is also observed that intralaminar damage is responsible for almost half of the total impact energy, followed by delaminations and friction. Stacking sequences with upper layers at 45° exhibit slightly higher energy dissipation due to intralaminar damage (fibre failure) and interlaminar damage (delamination).

Keywords: Asymmetric composites; Damage characterization; Numerical modelling; Impact response.

1. Introduction

Nowadays, composite materials are increasingly replacing traditional metallic materials due to the enormous benefits that can be obtained from their application. This is the result of their exceptional performance in terms of fast manufacturing, competitive cost, superior static and dynamic characteristics, high specific strength and stiffness, and good corrosion resistance [1–4]. In addition, their low weight allows for significant reductions in fuel consumption, which makes them particularly attractive from an energetic point of view.

Despite all the advantages reported, its application is still compromised in many applications due to the low resistance throughout the thickness. In fact, they prove to be particularly sensitive to low-velocity impacts, events that commonly occur in service or maintenance activities and promote damages that are difficult to detect visually [5, 6]. Apart from matrix cracking, fibre fracture and fibre–matrix debonding, delamination is one of the most important failure mechanisms because they drastically affect the residual properties of composite materials. For example, in terms of tensile strength, the literature reports reductions of between 16% and 25% due to the degradation of the fibre/matrix interface and stress concentration promoted by the delaminations [7–10]. Regarding the bending properties, reductions of between 34% and 78% can be found, depending on the position of the delamination along thickness and the layup sequence (symmetrical or anti-symmetrical layups) [11–13]. Finally, compressive strength can be reduced by around 60% due to the multiple delaminations that interact during compression and grow rapidly under buckling loads [14–18]. Amaro et al. [19], for example, developed a detailed study on the residual impact strength of carbon/epoxy laminates after bending and concluded that the magnitude of the initial damage has a determinant influence on the impact response of the laminates.

However, most of the studies available in the literature do not address asymmetrical laminates due to the decrease in performance caused by in-plane and out-of-plane interactions. Due to these interactions, distortion can occur during the curing process, which increases the stress levels and decreases the load-carrying capacity. However, these negative aspects of performance are rarely assessed accurately or included in the design process, which is why most of the studies available in the literature focus essentially on symmetrical laminates.



The studies performed by Sasikumar et al. [20–22] are an exception, in which the authors demonstrate that asymmetrical laminates can be a good solution, compared to symmetrical ones, for structural applications in the aeronautical field. In their first study [20], the authors proposed an asymmetrical laminate with ply clustering on the impact face of the laminate, which was compared with a laminate with a similar configuration, but, in this case, the ply clustering is on the non-impacted side. With this clustered ply block, the authors intend to induce high interlaminar shear stresses, which cause delamination at the interface at the corresponding ply interface and, consequently, promote delaminations at pre-determined regions. Based on experimental and numerical analyses, the authors concluded that, when the ply clustering is located on the impact face of the laminate, better resistance to damage is obtained. Compared to the laminate with ply clustering on the non-impacted side, benefits of around 30% were obtained in terms of threshold load for delamination and the projected delamination area was 20% lower for low-impact energies. The reason for this improvement was due to intralaminar damage, which is the most significant damage mechanism for laminates with clusters at the non-impacted side, causing a larger energy dissipation than delamination. Therefore, stacking sequences can be adapted according to the stress states expected in given load cases. Subsequently, the authors combined the concepts of asymmetry and ply hybridization into a laminate design, in which thick plies can be mixed with thin plies to form a hybrid laminate [21]. Moreover, the thicker plies can be positioned where desired without raising concerns about positioning similar thick plies over the laminate's midplane symmetry line. With this methodology, authors obtained about 50% and 30% reduction in terms of damage area and dissipated energy, respectively, over the thin-ply laminates. In addition to greater impact strength, the compressive strength after impact was also improved by around 30% compared to that observed for thin-ply laminates. This study allowed the authors to demonstrate that it is possible to mitigate the weakness of thin plies against impact and post-impact loads in an economical way. Finally, the authors studied three asymmetrical laminates, in which the local ply clusters were placed on the impact side, in the middle of the laminate and on the non-impacted side and compared the results with those obtained for a symmetric laminate (with no ply clusters) [22]. With this study, the authors proved that damage can be imposed at the desired locations through the design of the laminate. Furthermore, the asymmetric laminate with middle ply clusters increased the compressive strength after impact by 10% compared to the other configurations with ply clusters and buckled less, although having less impact resistance than the symmetric laminate. Therefore, this strategy can be an optimal solution for application to aircraft skins.

Based on the above benefits and because research into cylindrical shells is extremely important due to the increasing use of complex structures, this study aims to characterise the damage in asymmetrical semicylindrical composite laminate shells subjected to low-velocity impact loads. In fact, most of the works available in the literature report studies of flat plates subjected to low-velocity impacts and, in the case of semicylindrical composite laminates, although they are scarce, they focus on the influence of geometric parameters, boundary conditions and different materials/layup configurations [23–26]. More specifically, determining the energy dissipation mechanisms that occur during low-velocity impact events, as well as predicting and analysing the types of intralaminar and interlaminar damage, are the main objectives of this work. The intention is to continue the studies of Sasikumar et al. [20–22] but for semicylindrical composite laminated shells using, for this purpose, a numerical approach already validated in previous work developed by the authors [13, 27–29]. For this purpose, and maintaining the overall number of layers, authors used the following stacking sequences [0₄,45₄], [0₆,45₂], [0₇,45₁], [45₄,0₄], [45₆,0₂] and [45₇,0₁] to group layers with different numbers of constituents located on the impact and non-impact faces, with the aim of imposing delaminations at different specific locations throughout the thickness. The results will be discussed with each other and compared with the same symmetric configuration.

2. Numerical Model

This section provides an overview of the constitutive models used in the Finite Element (FE) simulations to evaluate the damage obtained in asymmetric curved composite laminates subjected to low-velocity impacts. These models were integrated into the study using ABAQUS/Explicit FE software [30]. They were defined based on previous numerical models developed for composite laminate shells reinforced with E-glass plain-weaved fabrics [23, 27–29]. It should be noted that the experimental evidence presented in [25] served as the basis for this study. In this way, the composite semicylindrical shells were manufactured through resin transfer moulding, with an internal radius of 50 mm, a length of 100 mm, and an average thickness of 2.53 mm. These shells comprise of eight layers of woven carbon fibre fabric (160 g/cm², plain-weave), sourced from Composite Materials Italy (CIT), with SR1500 epoxy resin and SD2503 hardener, both provided by Sicomin (Châteauneuf-les-Martigues, France). Figure 1 presents the experimental setup employed, including the testing equipment and specimen support device, nevertheless, more details about the experimental procedure can be obtained in [25].

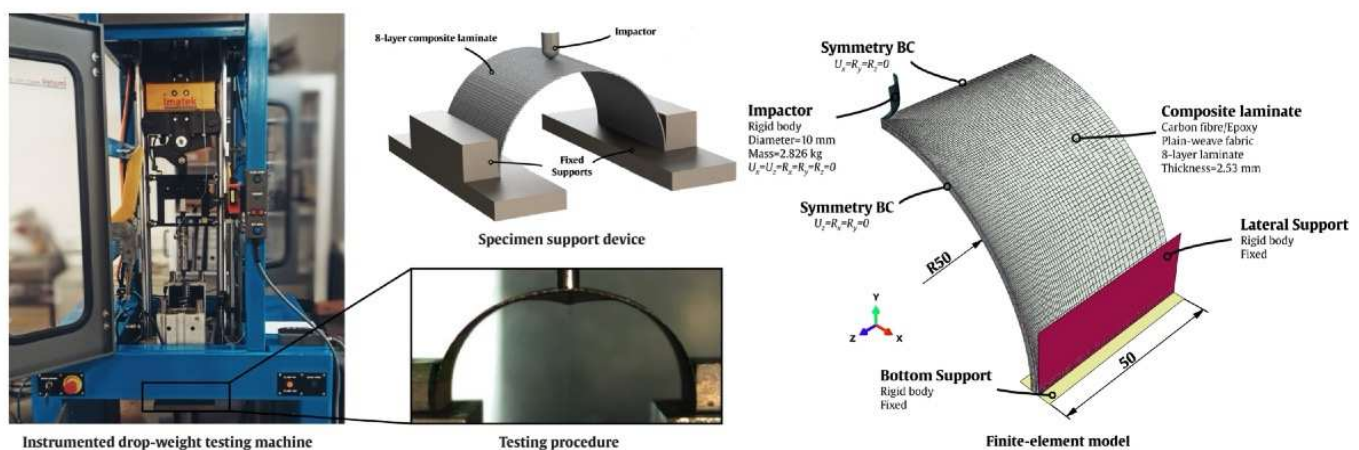


Fig. 1. Experimental setup and generated FE model of a semicylindrical composite shell.



Table 1. Intralaminar stiffness and strength properties of the composite layers.

Description	Symbol	Units	Value
Density	ρ	kg/m ³	1600
Young's modulus	$E_1 = E_2$	GPa	69
Poisson's ratio	ν_{12}	-	0.04
In-plane shear modulus	G_{12}	GPa	7.1
Tensile strength	$X_{1+} = X_{2+}$	MPa	640
Compressive strength	$X_{1-} = X_{2-}$	MPa	540
Shear strength	S	MPa	180

Table 2. Damage evolution parameters and shear plasticity coefficients.

Description	Symbol	Units	Value
Maximum shear damage	d_{12}^{max}	-	1
Shear damage parameter	α_{12}	-	0.3221
Initial effective shear yield stress	$\tilde{\sigma}_{y0}$	MPa	80
Coefficient in hardening equation	C	-	788
Power term in hardening equation	p	-	0.552

2.1. Finite Element Discretization

The woven fabric layers were modelled using continuum shell elements (SC8R) that incorporate reduced integration and a stiffness hourglass formulation. For the impactor, discrete rigid elements (R3D4) were employed, while the supports were modelled as analytical rigid bodies. To strike a balance between computational efficiency and numerical prediction accuracy, it was crucial to optimize the FE mesh discretization, especially in the vicinity of the impact region. For this purpose, a seeding strategy was applied along both the curved and straight edges of the semicylindrical shell, increasing the FE mesh density precisely in the impact region. Simultaneously, the mesh density was reduced progressively beyond this critical area. The FE mesh discretization used in this study is shown in Fig. 1.

The 8-layer FE model generated for this study consists of 48,000 linear hexahedral elements of type SC8R and 949 linear quadrilateral elements of type R3D4. A seeding strategy was implemented, leading to a variation in element size across the laminas. Within the impact region, elements with an approximate global size of 0.3 mm were applied, progressively expanding to 2 mm in regions farther from the impact zone. Irrespective of the stacking sequence under examination, a consistent FE mesh discretization was adopted, featuring identical characteristic length and aspect ratio in all simulations. This method guarantees the comparability of predictions across diverse stacking sequences. To expedite solution computations a semi-automated uniform mass scaling strategy was implemented. To prevent any influence of mass scaling on the results, it is essential to keep the kinetic energies resulting from the mass scaling effect below 5 to 10% of the total internal energy [30]. Therefore, in this study, the kinetic energies account for less than 3% of the total internal energy.

2.2. Boundary Conditions

The FE model considers the geometrical characteristics of the specimens examined in [25]. These specimens present a semi-circular cross-sectional shape with an internal radius of 50 mm and a length of 100 mm, as shown in Fig. 1. They consist of 8 composite fabric layers, resulting in a composite thickness of 2.53 mm. To accurately simulate the experimental setup, two fixed rigid body supports were added: a lateral support and a bottom support. Moreover, to optimize computational efficiency, the FE model exploited geometric symmetries, focusing on one-quarter of the composite shell. Symmetry boundary conditions were imposed on the plane parallel to the yz-plane and one of the surfaces parallel to the xy-plane, as depicted in Fig. 1. The impactor used in the simulations had a lumped mass of 2.826 kg with a hemispherical head of 10 mm diameter. An impact velocity of 1.88 m/s was chosen to match the 5 J impact energy used in the experimental campaign [25]. Additionally, all rotational degrees of freedom of the impactor were constrained, allowing only displacements along the y-axis.

2.3. Intralaminar Properties

A Continuum Damage Model (CDM) was used to model the intralaminar damage within the ABAQUS/Explicit [30]. This model was implemented using the integrated VUMAT subroutine ABQ_PLY_FABRIC, developed by Johnson et al. [31], which is based on the Ladeveze and LeDantec damage model [32]. This subroutine is designed for compatibility with plane-stress elements and treats each woven fabric-reinforced lamina as an orthotropic elastic material. The material's structural integrity degrades due to factors such as fibre failure, matrix cracking, and plastic deformation under shear-loading conditions. It utilizes the maximum stress failure criterion to identify the onset of damage within the fibres and incorporates a damage evolution model based on fracture energies to govern the subsequent reduction in stiffness. Detailed information about this constitutive model is available in [27–29]. The constitutive material model implemented requires the definition of the laminae stiffness and strength properties, in both the longitudinal and transverse directions of the fibres. The intralaminar material properties values were approximated from the results presented by Hou and Ruiz in [33], and are shown in Table 1.

The coefficients governing the evolution of damage are determined based on the fracture energies associated with tensile and compressive loading in both the longitudinal and transverse directions of the fibres (denoted as G_f^{1+} , G_f^{1-} , G_f^{2+} and G_f^{2-}). Additionally, these coefficients depend on parameters d_{12}^{max} and α_{12} . As for the coefficients governing shear plasticity, they encompass the initial effective shear yield stress $\tilde{\sigma}_{y0}$ and the values of C and p . These parameters and coefficients are determined through the experimental procedure detailed in [34]. However, considering the intricacy of the experimental procedure, these coefficients were estimated from [27–29] and a preliminary parametric study was performed to adjust them to the experimental evidence. It should be noted that given the structural characteristics of the woven fabric reinforcement (plain weave), the fracture energies associated with both the longitudinal and transverse directions were assumed to be equivalent. In this way, a value of 2000 J/m² was defined for the fracture energies. A similar procedure was implemented for the damage evolution parameters d_{12}^{max} and α_{12} , and the shear plasticity coefficients, $\tilde{\sigma}_{y0}$, C and p . The values employed are presented in Table 2.



Table 3. Interlaminar properties.

Description	Symbol	Units	Value
Cohesive stiffness	$K_{nn} = K_{ss} = K_{tt}$	N/mm ³	10 ⁶
Maximum nominal stress	$\tau_n^0 = \tau_s^0 = \tau_t^0$	MPa	73
Fracture energy	$G_n^c = G_s^c = G_t^c$	J/m ²	300
Interaction parameter	η	-	1.45

2.4. Interlaminar Properties

In the context of the current study, a stress-based criterion was employed for the traction-separation response. In this way, the elastic behaviour of the cohesive surfaces can be expressed as:

$$\tau = K\varepsilon \Leftrightarrow \begin{Bmatrix} \tau_n \\ \tau_s \\ \tau_t \end{Bmatrix} = \begin{bmatrix} K_{nn} & 0 & 0 \\ 0 & K_{ss} & 0 \\ 0 & 0 & K_{tt} \end{bmatrix} \begin{Bmatrix} \varepsilon_n \\ \varepsilon_s \\ \varepsilon_t \end{Bmatrix} \quad (1)$$

where τ denotes the nominal stress tensor, ε represents the nominal elastic strain tensor, and K corresponds to the elasticity matrix. The subscripts n , s , and t are used to specifically designate the normal and shear directions, respectively. It should be noted that the off-diagonal elements in the elasticity matrix are zero, as there is no coupling behaviour between the normal and shear components. The initial linear response, effective until damage initiation occurs, is controlled by the prescribed values of cohesive stiffness: K_{nn} for the normal direction, and K_{ss} and K_{tt} for the shear directions. In the present study, the cohesive stiffness is set to 10⁶ N/mm³, following the recommendation of Camanho et al. [35]. Additionally, it is assumed that this value remains consistent across all directions, i.e., $K_{nn} = K_{ss} = K_{tt}$, a simplification that has been validated in several previous studies yielding satisfactory results [27–29, 36–38]. The quadratic failure criterion based on stress, as represented in Eq. (2), is utilized to anticipate the initiation of damage. In this equation, τ_n , τ_s , and τ_t stand for the normal and shear contact stresses at the interface, while τ_n^0 , τ_s^0 , and τ_t^0 represent the peak values of the nominal stress. It's worth noting that the Macaulay brackets $\langle \cdot \rangle$ signify that compressive stress does not initiate damage:

$$\left(\frac{\langle \tau_n \rangle}{\tau_n^0} \right)^2 + \left(\frac{\tau_s}{\tau_s^0} \right)^2 + \left(\frac{\tau_t}{\tau_t^0} \right)^2 = 1 \quad (2)$$

Once the damage initiation is reached, characterized by the quadratic interaction function reaching a value of 1, the cohesive stiffness experiences degradation. Equation (3) delineates the progressive weakening of the cohesive surface. The variable D denotes the scalar damage coefficient that represents the overall damage in the material. Furthermore, $\bar{\tau}_n$, $\bar{\tau}_s$ and $\bar{\tau}_t$ represent the stress components predicted by the elastic traction-separation behaviour without damage:

$$\begin{aligned} \tau_n &= (1 - D)\bar{\tau}_n, \text{ with } \bar{\tau}_n \geq 0 \\ \tau_s &= (1 - D)\bar{\tau}_s \\ \tau_t &= (1 - D)\bar{\tau}_t \end{aligned} \quad (3)$$

The fracture energies define the evolution of the damage coefficients from the initiation of damage to ultimate failure. The calculation of fracture energy G^c adheres to the Benzeggagh and Kenane (B-K) criterion under mixed-mode loading [39], as expressed in Eq. (4), and assuming that the critical fracture energies during deformation along shear directions t and n , are identical:

$$G^c = G_n^c + (G_s^c - G_n^c) \left(\frac{G_s}{G_T} \right)^\eta, \text{ with } G_S = G_s + G_n \text{ and } G_T = G_n + G_s \quad (4)$$

In this equation, G_n and G_s signify the work done by the traction in the normal and shear directions, while G_n^c and G_s^c represent the critical strain energy release rates required to cause failure in the normal and shear directions. The parameter η is an interaction parameter within this context. The interlaminar properties utilized in this study are detailed in Table 3. The values for the maximum nominal stress $\tau_n^0 = \tau_s^0 = \tau_t^0$ and fracture energy $G_n^c = G_s^c = G_t^c$ were obtained from [40, 41]. Furthermore, the interaction parameter η was the one adopted in [27, 28].

2.5. Contact Interactions

A penalty enforcement contact methodology was used to simulate surface-to-surface interactions between the composite shell, impactor, supports, and interfaces between laminas. Friction coefficients were specified for different contact pairs, considering the nature of the materials and interfaces. The friction coefficient values, denoted as μ , pertinent to metal-composite contacts and fully delaminated interfaces, were obtained from literature. Subsequently, a value of $\mu = 0.3$ was specified for the contact between the hemispherical head of the impactor and the upper surface of the composite laminate. Furthermore, a value of $\mu = 0.7$ was employed to describe the interaction between the support surfaces and the composite laminate surfaces. The friction coefficient at the interface between the layers was set to $\mu = 0.5$.

3. Validation of the Numerical Model

The validation process presented in this section involves a direct comparison between the numerical predictions and the experimental results described in [25]. The specimens used in the experimental tests had eight woven fabric layers stacked in a single direction, with the warp or weft direction aligned parallel to the semicylindrical axis. This stacking sequence will be denoted as $[0]_8$. Notice that the validation of the numerical model is crucial to ensure its accuracy and reliability. To achieve this, the model's predictions were compared with experimental data obtained from symmetric specimens, which served as a benchmark for assessing its performance. Despite the asymmetry introduced in subsequent analyses, the key parameters maintained their uniformity across the asymmetrical FE models. This included preserving identical geometric configurations, boundary conditions, and material properties, ensuring a consistent basis for comparison and evaluation.



Table 4. Asymmetric stacking sequences analysed.

Stacking Sequence	Simplified notation
(0/0/0/0/45/45/45/45)	[0 ₄ ,45 ₄]
(0/0/0/0/0/0/45/45)	[0 ₆ ,45 ₂]
(0/0/0/0/0/0/0/45)	[0 ₇ ,45 ₁]
(45/45/45/45/0/0/0/0)	[45 ₄ ,0 ₄]
(45/45/45/45/45/0/0/0)	[45 ₆ ,0 ₂]
(45/45/45/45/45/45/0/0)	[45 ₇ ,0 ₁]

To assess the model's accuracy, the numerical and experimental force-time and energy-time curves are analysed, as shown in Fig. 2(a). It is evident that the numerical predictions exhibit a satisfactory agreement with the experimental evidence across the force and energy history curves. The maximum force, a parameter that is often associated with the impact's peak load-bearing capacity, shows a satisfactory numerical-experimental correlation. Although the numerical prediction indicates a slightly lower value, this deviation is within an acceptable error margin of around 8.5%. The elastic energy, which represents the energy absorbed by the material up to the point of maximum impact force, exhibits good agreement with negligible error. It can be seen in Fig. 2(b) that the total energy, as indicated by the ABAQUS/Explicit output ETOTAL, remains stable throughout the simulation, reflecting the proper definition of time increments. Furthermore, the ratio between the artificial strain energy (ALLAE output) and internal energy (ALLIE output) reaffirms the appropriateness of the hourglass control method that was implemented.

In summary, although small deviations are noticeable in the context of maximum force, the overall alignment between FE model's predictions and the impact response of the semicylindrical composite shells tested is indicative of the effectiveness and reliability of the FE model.

4. Results

In this section, numerical predictions related to the impact response of curved laminated composites involving asymmetrical stacking sequences are presented and discussed. For this purpose, eight woven fabric layers are placed in two different directions, specifically 0° and 45° in relation to the semicylindrical axis, and the configurations analysed are shown in Table 4. Furthermore, to compare the impact performance of asymmetrical and symmetrical laminates, the results are juxtaposed with those obtained for the symmetric laminate sequence [0₈], validated in Section 3.

The numerically predicted force-time and force-displacement curves for the stacking sequences presented in Table 4 are depicted in Fig. 3. For all the configurations analysed, it is possible to observe a response that is typical of curved laminates when subjected to low-velocity impact loads. To be more specific, the profile of the curves is characterized by an increase in force up to a maximum value, P_{max}, after which there is a more or less abrupt drop. The P_{max} value, which is strongly influenced by the impact energy, establishes the maximum load that a composite laminate can resist before being seriously damaged. The behaviour described above is perfectly in line with that observed in other studies reported in the literature [23, 25, 42-44], where the oscillations seen in the curves are caused by the elastic wave and the vibrations of the samples [45, 46]. Furthermore, because the impactor constantly returns, the impact energy is insufficient to encourage full penetration and, in this context, all the laminates were affected by a non-perforating impact. Figure 4 confirms this highlight, where the loss of contact between the striker and the sample corresponds to the beginning of the curve's plateau [47]. This energy corresponds to the energy absorbed by the specimen, and the elastic energy (restored energy) can be estimated as the difference between the absorbed energy and the energy at peak load [48].

Therefore, for a clearer understanding of the placement of the 0° or 45° layers in the top/bottom half of the composite shells, Fig. 5 directly compares configurations [0₄,45₄] and [45₄,0₄], while Table 5 summarizes the results of all configurations.

In general, the overall impact responses of all laminates are quite similar, which is in line with the study developed by Sasikumar et al. [22]. However, a more detailed analysis shows that, in terms of maximum impact force, it decreases as the number of layers at 0° increases and when they are placed in the upper half of the curved laminate. For example, the maximum impact force decreases by around 11.3% when comparing the values obtained between [0₄,45₄] and [0₇,45₁]. On the other hand, curved laminates with the top layers in a 45° direction are characterized by a fluctuation in the maximum impact force around an average value of 2.03 kN, but when the [45₄,0₄] configuration is compared with the similar 0° configuration ([0₄,45₄]), the impact force is 6% higher. Therefore, according to Sasikumar et al. [22], different delamination threshold loads are expected and, consequently, damages of different severity.

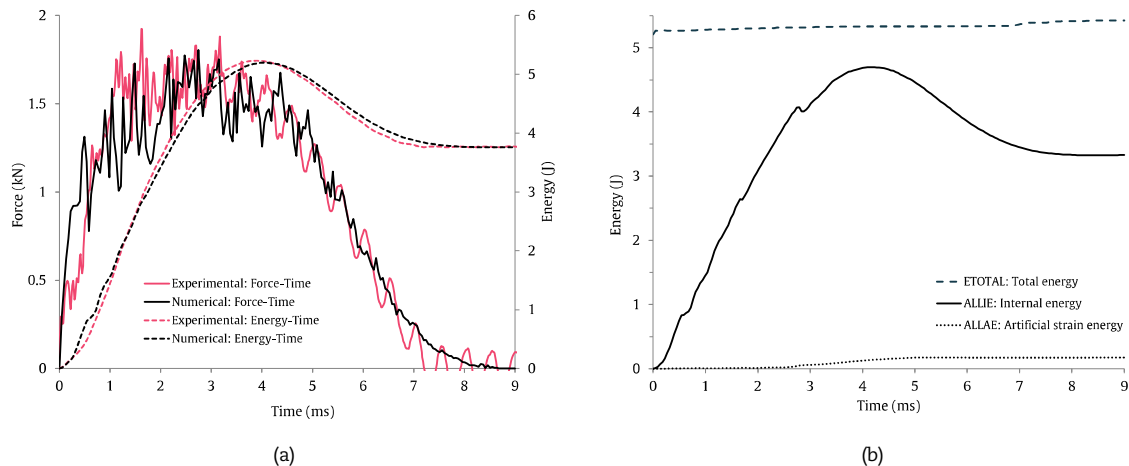


Fig. 2. Validation of the numerical model for a [0]₈ composite shell: (a) Experimental and numerical force and energy histories, (b) Total energy, internal energy, and artificial strain energy histories.



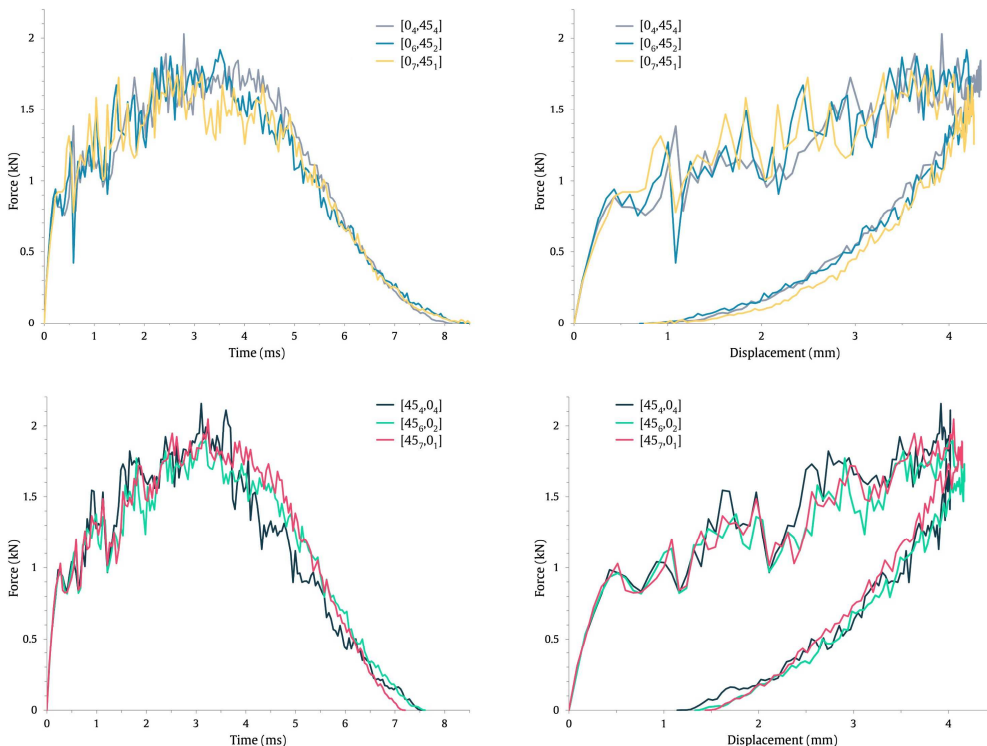


Fig. 3. Numerical predicted force-time and force-displacement results for the asymmetric stacking sequences.

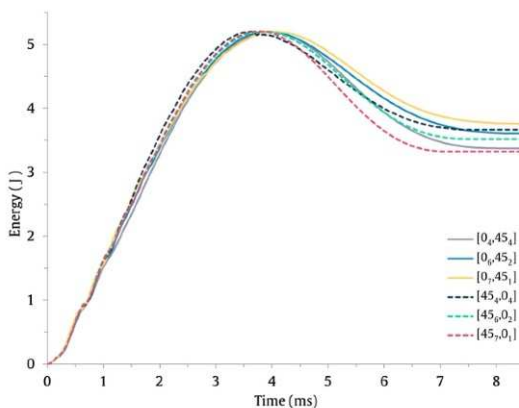


Fig. 4. Numerical predicted energy-time results for the asymmetric stacking sequences.

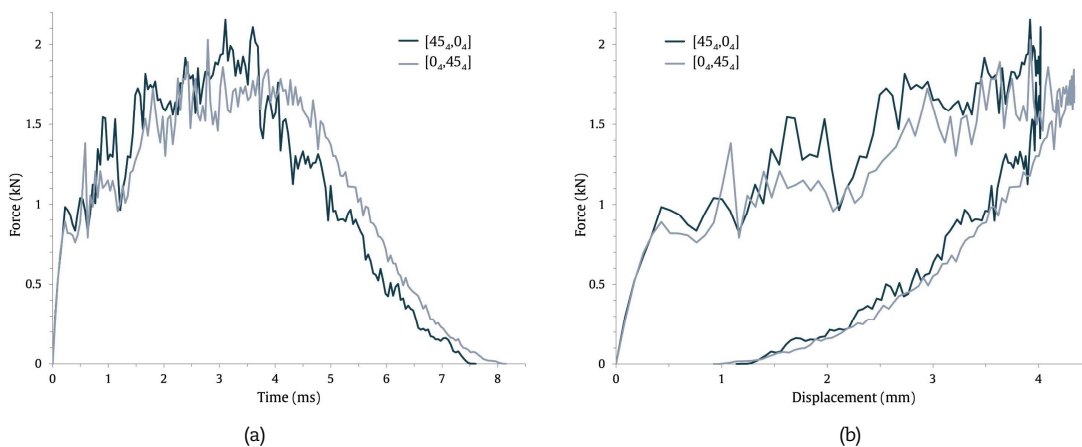


Fig. 5. Numerical predicted force-time and force-displacement results for the asymmetric stacking sequences $[0_v, 45_v]$ and $[45_v, 0_v]$.



Table 5. Maximum force, maximum displacement, contact time and absorbed energy for the analysed stacking sequences.

Stacking sequence	Maximum		Contact Time (ms)	Absorbed Energy (J)
	Force (kN)	Displacement (mm)		
[0 ₄ ,45 ₄]	2.03	4.33	8.15	3.37
[0 ₆ ,45 ₂]	1.92	4.23	8.51	3.60
[0 ₇ ,45 ₁]	1.80	4.27	8.73	3.76
[45 ₄ ,0 ₄]	2.15	4.02	7.61	3.67
[45 ₆ ,0 ₂]	1.89	4.17	7.61	3.52
[45 ₇ ,0 ₁]	2.05	4.15	7.20	3.32
[0 ₈]	1.80	4.27	8.73	3.76

Regarding the impact displacement, both configurations fluctuate around different average values, which are about 4.28 mm for curved laminates with a 0° orientation placed on the top layers and 4.11 mm when the top layers are at 45°. However, all configurations with the 45° orientation at the top have lower displacement values than those with the 0° orientation. For example, the displacement is around 7.2% lower when comparing the values obtained between [0₄,45₄] and [45₄,0₄]. Considering the estimated contact time, it is higher for the curved laminates with the 0° direction at the top, reaching a difference of 7.1% between [0₄,45₄] and [45₄,0₄]. On the other hand, while increasing the layers at 0° at the top of curved laminates leads to an increase in contact time, the opposite occurs for laminates at 45°. It is observed that between [0₄,45₄] and [0₇,45₁] the increase is around 7.2%, while between [45₄,0₄] and [45₇,0₁] the decrease is about 5.4%.

Finally, the trend observed for the absorbed energy is similar to that of the contact time, but when comparing the configurations [0₄,45₄] and [45₄,0₄] the absorbed energy in the first case is around 8.2% lower. In this case, the increase between [0₄,45₄] and [0₇,45₁] is around 11.6%, while between [45₄,0₄] and [45₇,0₁] the decrease is around 9.5%, with the particularity of the absorbed energy being very similar between the configurations [0₄,45₄] and [45₇,0₁]. Therefore, because the absorbed energy is related to the severity of the damage [47,49], and according to Sasikumar et al. [20] this type of laminates has several delaminated interfaces, although one is dominant (the one that governs the total delamination profile and plays a dominant role in the damage tolerance of the structure), a detailed analysis of the damage mechanisms will be developed for each laminate and related to the absorbed/dissipated energy.

For this purpose, an analysis of the energy absorption/dissipation mechanisms linked to low-velocity impacts on asymmetric semicylindrical composite shells is presented. In contrast to unlike experimental tests, the generated FE models offer the capability to quantify energy absorption across multiple mechanisms. These mechanisms encompass the intralaminar damage, accounting for energy dissipation resulting from fibre damage, interlaminar damage, reflecting the energy dissipation due to delamination, and friction which encompasses various interactions, including those between the rigid impactor and the composite shell, as well as interactions within the delaminated layers. The contribution of each of the energy-absorption mechanisms for the various asymmetric stacking sequences and the symmetric [0₈] stacking sequence are presented in Fig. 6. Notice that the energy dissipation mechanisms were identified by analysing specific ABAQUS outputs: intralaminar damage (represented as ALLPD - Plastic dissipation), interlaminar damage (ALLDMD - Damage dissipation), and frictional effects (ALLFD - Frictional dissipation).

Overall, a clear pattern emerges where most of the energy absorption occurs through intralaminar damage (comprising 48.7% to 57.5%), followed by delamination (ranging from 32.8% to 38.4%), and friction (falling within the 7.1% to 15.5% range). These results are consistent with the numerical predictions of the low-velocity impact response of asymmetric composites presented by Sasikumar et al. [20]. These authors also identified fibre failure (intralaminar damage) as the main energy dissipation mechanism. It is worth noting that the contribution of artificial strain energy dissipation remains minimal and consistently below 2% of the total impact energy across all stacking sequences. This consistency underscores that the results remain unaffected by this factor [30].

According to Fig. 6, in stacking sequences where the upper layers are oriented at 45°, there is a marginally greater energy dissipation attributed to fibre failure (intralaminar damage) and delamination when compared to those with a 0° orientation. In the first set of configurations ([45₄,0₄], [45₆,0₂] and [45₇,0₁]), intralaminar damage accounts for a range of 48.7% to 51.1%, while delamination constitutes between 37.9% to 32.8% of the overall energy dissipation. Conversely, for the second set ([0₄,45₄], [0₆,45₂] and [0₇,45₁]), the values exhibit variations between 53.2% and 57.5% for intralaminar damage, and 32.8% to 38.4% for delamination. Furthermore, it can be observed that energy dissipated by these damage mechanisms (intralaminar damage and delamination) are not substantially affected by the changes in the stacking sequence in the lower half of the stacking sequence.

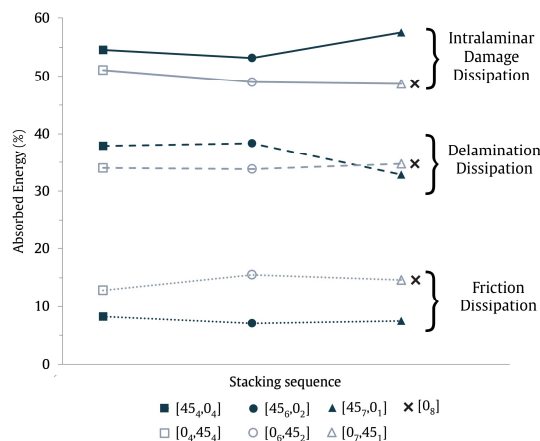


Fig. 6. Contribution of various energy-absorption mechanisms: intralaminar damage, delamination, and friction.



The $[45_7,0_1]$ configuration exhibits a noteworthy increase in intralaminar damage and a corresponding decrease in interlaminar damage compared to other configurations. According to Classical Laminate Theory, any alteration in the fibre orientation angle induces variations in the laminate's apparent in-plane stiffness properties. Specifically, the increase of 45° laminas in the laminate configuration leads to a reduction of the in-plane elastic modulus and an increase of the in-plane shear modulus, thereby influencing the impact response of the laminates and subsequently the mechanisms governing energy dissipation [13]. This phenomenon may elucidate the observed increase in intralaminar damage percentage and decrease in interlaminar damage for the $[45_7,0_1]$ configuration. Furthermore, a supplementary study revealed that if a stacking sequence with $[45_8]$ is considered, there is a slight increase in the percentage of energy absorbed by intralaminar damage and a corresponding slight decrease in interlaminar damage compared to the latter configuration. This underscores the impact of apparent in-plane stiffness properties on the impact performance of composite shells.

Friction accounts for the lowest energy dissipation among the mechanisms. Nevertheless, its significance should not be understated, as it still constitutes up to about 15% of the total dissipated energy. This value is in good agreement with the findings presented by Lopes et al. [50]. These authors developed a numerical analysis of low-velocity impact damage in dispersed stacking sequence composite laminates, and their study similarly indicated that friction constitutes the mechanism with the least energy dissipation, accounting for approximately 15% of the total impact energy. Furthermore, it is evident that frictional dissipation is more pronounced in asymmetric laminates with the upper layers aligned at 0° , with values ranging from 12.9% to 15.5%. On the other hand, for stacking sequences with the upper layers aligned at 45° , the frictional dissipation values range from 7.1% to 8.2%. Once again, it is apparent that altering the alignment of the bottom layers has a negligible impact on the energy dissipated through friction.

As it is possible to appreciate in Table 5, the results highlight a similarity in the predicted impact behaviour between the symmetric laminate $[0_8]$ and the asymmetric laminate $[0_7,45_1]$, in terms of maximum force, maximum displacement, contact time, and absorbed energy. Additionally, it was observed that the contributions of the energy absorption mechanisms (intralaminar damage, delamination, and friction) for these two laminate configurations are also comparable, as illustrated in Fig. 6. This similarity reinforces the previous discussed findings in which, for the analysed stacking sequences and load conditions, the orientation of the bottom layers has a negligible effect on the laminate's performance.

Considering that intralaminar damage accounts for the most substantial portion of energy dissipation, an analysis was carried out to determine the layers that contribute the most to this dissipation. Consequently, the energy dissipated by intralaminar damage for each layer within various asymmetric stacking sequences and the symmetric $[0_8]$ stacking sequence are presented in Fig. 7.

The results show that the amount of energy dissipated by intralaminar damage decreases, steadily in general, from the top to the bottom layers across all considered stacking sequences, agreeing with what was observed by Sasikumar et al. [20]. These results were expected, as when there is no puncturing in the specimens, fibre damage predominantly occurs in layers that are in closer contact with the impactor [23]. It is possible to observe that the first layer of stacking sequences $[45_4,0_4]$ and $[0_4,45_4]$ exhibits the highest (18.8%) and lowest (15.3%) energy dissipation, respectively. Moreover, the top four layers of stacking sequence $[45_4,0_4]$ dissipate about 17.3% more energy than their counterparts in $[0_4,45_4]$. On the other hand, the opposite trend emerges for the bottom four layers, with $[0_4,45_4]$ demonstrating approximately 30% greater energy dissipation than $[45_4,0_4]$. A significant drop in energy dissipation in stacking sequence $[45_4,0_4]$ is particularly evident between layer 4 and 5, corresponding to the shift in the woven fabric's alignment from 45° to 0° . These results underscore that the distribution of energy dissipated by intralaminar damage is influenced by layer positioning and orientation. Placing layers oriented at 45° either in the upper or lower half of the specimen results in increased energy dissipation compared to those oriented at 0° . While as mentioned before, the general trend across all configurations indicates a decrease in the energy dissipated by intralaminar damage from top to bottom layers, certain stacking sequences exhibit a slight deviation. Notably, some configurations show an increase in energy dissipation at positions 6 and 8. For instance, in Fig. 7, layer 6 of stacking sequence $[0_4,45_4]$ the percentage of energy dissipated by intralaminar damage rises from 12.7% at layer 5 to 14% at layer 6. There appears to be no discernible correlation between layer orientations and their positions that could explain this subtle yet sudden increase. Further investigation is warranted to elucidate the underlying factors contributing to this phenomenon.

In the case of the remaining asymmetric stacking sequences, where the number of layers oriented at 0° and 45° gradually increases within the lower half of the laminate thickness, the results reveal a more uniform decline in energy dissipation when compared with $[45_4,0_4]$ and $[0_4,45_4]$. Furthermore, no trend emerges from the change in the layer's orientation, as the stacking sequences exhibit comparable distributions of energy dissipated by intralaminar damage. As depicted in Fig. 7, the energy dissipation caused by intralaminar damage in each layer exhibits a consistent pattern across both the asymmetric stacking sequence $[0_7,45_1]$ and the symmetric stacking sequence $[0_8]$.

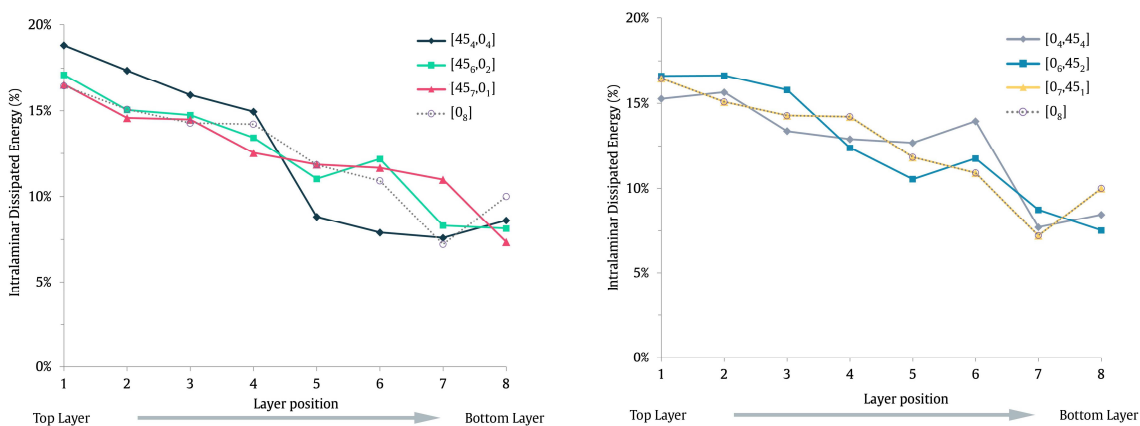


Fig. 7. Energy dissipated by intralaminar damage in each layer for the analysed stacking sequences.



To complement the preceding findings, Fig. 8 presents the intralaminar damage predicted by the numerical models. It is important to observe that the depicted damage results from the interplay of tensile and compressive fibre failures along both directions of the woven fabric, as well as shear damage. The diverse orientations of the failed fibres are distinctly discernible across the semicylindrical composite shells, aligning with the asymmetric stacking sequences of the laminates.

In terms of intralaminar damage dissipation, it becomes evident that stacking sequences with the upper layers (the impact side) oriented at 45°, as depicted in Fig. 6, exhibit higher levels of damage. This observation suggests that these laminate configurations experience a more extensive degree of damage resulting from fibre failure. It's important to note that these differences in damage extent among the asymmetric stacking sequences are not easily discernible in Fig. 8. However, a distinct pattern emerges when considering the projected intralaminar damaged area in relation to the stacking sequence. For instance, when examining stacking sequences [45₄,0₄], [45₆,0₂] and [45₇,0₁], it is noticeable that the predicted intralaminar damaged region decreases as the number of layers at 45° increase. However, the energy dissipated by this mechanism slightly increases, as shown in Fig. 6. These results imply that increasing the number of layers at 45° does not necessarily reduce the overall amount of intralaminar damage. Instead, it contributes to constraining the extent of the projected intralaminar damaged area around the impact point. For stacking sequences with the upper layers oriented at 0°, that is [0₄,45₄], [0₆,45₂] and [0₇,45₁], a similar trend is discernible. Increasing the number of layers oriented at 45° in these sequences serves to diminish the projected damaged area surrounding the impact point.

To demonstrate this evidence, Fig. 9 provides a visual representation of the delaminated areas within the asymmetric stacking sequences. It's worth noting that these results specifically pertain to fully delaminated interface nodes, which are nodes where the CSMG output has reached a value of 1. The delaminated area values shown in Fig. 9 are a cumulative sum of delaminated interface areas, and they do not reflect the projected area.

In all the stacking sequences, a typical low-velocity impact damage morphology is observed. This morphology is characterized by a spiral staircase delamination pattern, where the delaminations are more extensive in the lower interfaces and diminish towards the upper interfaces (side of impact) [29, 51, 52]. This pattern arises due to bending of the composite shell during the impact event, which consequently causes higher interlaminar shear stresses to appear on the lower interfaces. Nevertheless, it can be appreciated that the choice of stacking sequence can exert a significant influence on the total delaminated area, with differences reaching up to approximately 25.4%. This disparity is especially evident when comparing [45₄,0₄] and [45₇,0₁]. A notable reduction in the delaminated area is evident when comparing stacking sequences [45₆,0₂] to [45₇,0₁]. This can be attributed to higher interlaminar shear stresses developing on the lower interfaces and an increase in the number of layers at 45°, which cause an augmentation of the in-plane shear modulus of the laminate. Therefore, contributing to the reduction of delamination in the layers most affected by it. This dual effect underscores the complex interplay between laminate configuration, interlaminar stresses, and material properties in influencing delamination behaviour.

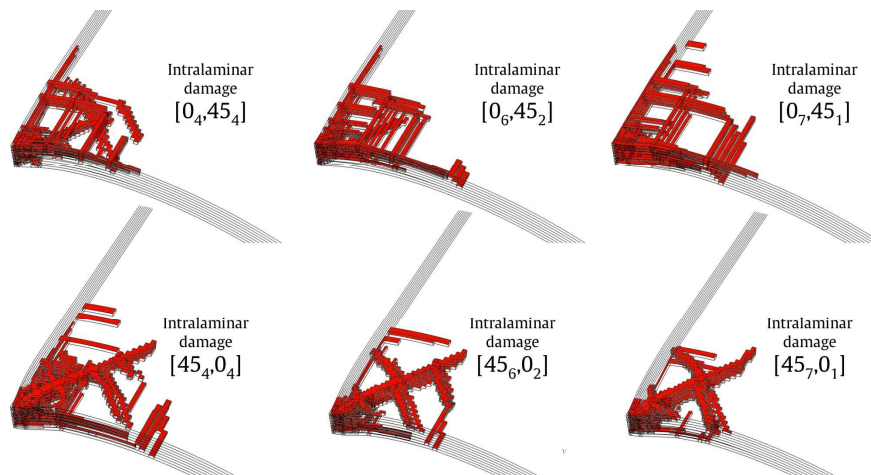


Fig. 8. Intralaminar damage for the asymmetric stacking sequences.

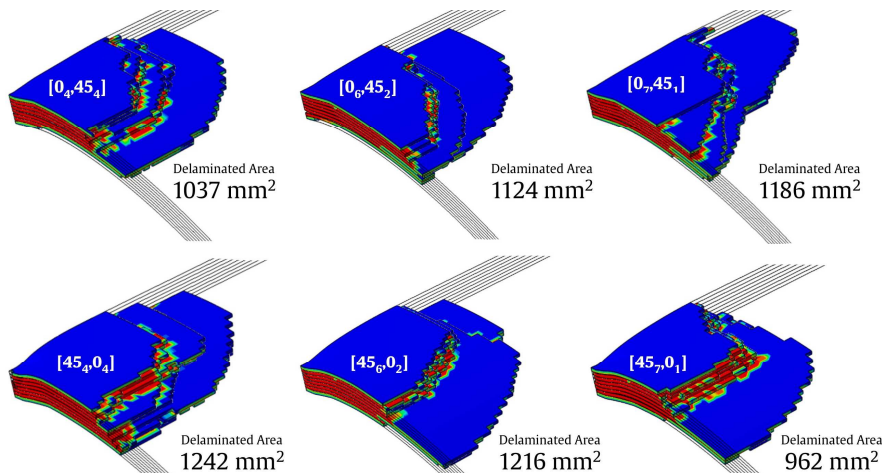


Fig. 9. Delaminated areas for the asymmetric stacking sequences.



In a broader context, and based on the stacking sequences analyzed, the results demonstrate a consistent trend wherein stacking sequences with upper layers oriented at 45° tend to promote delamination more than their counterparts with upper layers oriented at 0° . This observation aligns with the data presented in Fig. 6, which also showcases higher energy dissipation due to delamination for these stacking sequences. However, it's worth noting that there is an exception to this trend, observed in configurations $[0_7, 45_1]$ and $[45_7, 0_1]$, where the pattern is inverted. Once again, this divergence can be linked to the energy dissipation results found for these specific configurations in Fig. 6. These results are consistent with the conclusions reported by Sasikumar et al. [20] in their investigation of the impact response of nonsymmetric composite laminate plates. Identically, their research indicated that the positions of larger delaminations exhibit variation among different stacking sequences. Therefore, it is possible to intentionally induce damage, particularly delamination, at specific locations by the laminate stacking sequence, thus allowing for the customization of damage resistance. Comparable observations of controlled delamination were documented in [20, 22, 53, 54], employing laminate stacking sequence designs.

The use of asymmetrical stacking sequences can offer the potential for enhanced low-velocity impact damage resistance. In certain aerospace applications, the incorporation of asymmetrical composite laminates presents a potentially advantageous solution. They offer the versatility to serve as an option for designing laminates that are specifically tailored to withstand impact loads, complementing for example the hybrid laminate designs [21, 55]. In this context, the concept involves configuring the orientation of the layers so that the intralaminar damage region is controlled and/or the critical delamination damage is mitigated on a determinate position of the laminate.

5. Conclusion

This study utilised previously validated numerical models to characterize damage in asymmetric semicylindrical composite laminate shells subjected to low-velocity impact loads. The impact performance of asymmetric stacking sequences was assessed, comparing parameters such as force, displacement, contact time and absorbed energy. The use of 3D FE models in conjunction with a continuum damage mechanics model and a surface-based cohesive model allowed the possibility of taking into consideration the intralaminar and interlaminar damage. It was observed that the maximum force decreases as the number of layers oriented at 0° increases, particularly when these layers were placed in the upper half of the laminate. Displacement values vary for different configurations, with the lowest values for those with a 45° orientation in the top layers. On the other hand, the contact time was notably higher for laminates with a 0° orientation at the top. Regarding the absorbed energy, the trend observed was similar to that of contact time, with distinct variations between stacking sequences. Intralaminar damage contributed significantly to energy absorption, accounting for around half of the total energy dissipation, followed by delamination and friction. The energy dissipation attributed to intralaminar damage and delamination was slightly higher in the stacking sequences with the top layers oriented at 45° . Moreover, it was observed that increasing the number of layers at 45° constrained the extent of the damaged area around the impact point. On the other hand, interlaminar damage was significantly influenced by the stacking sequence. Those with upper layers oriented at 45° promote more delamination than similar ones with layers oriented at 0° . Therefore, this study highlighted the importance of selecting an appropriate stacking sequence to optimize the impact strength and manage damage characteristics in composite laminates. It has been proven that asymmetric stacking sequences offer the possibility of controlling intralaminar damage and minimizing critical delamination damage at specific locations within the laminate.

Author Contributions

The conceptualization of the study was led by L.M. Ferreira and P.N.B. Reis, while methodology development was a collaborative effort involving L.M. Ferreira, P.N.B. Reis, and C.A.C.P. Coelho; L.M. Ferreira was responsible for software implementation, and validation was conducted by L.M. Ferreira, P.N.B. Reis, and C.A.C.P. Coelho; Formal analysis was performed by L.M. Ferreira and P.N.B. Reis, with investigation efforts shared among L.M. Ferreira, P.N.B. Reis, and C.A.C.P. Coelho, L.M. Ferreira and P.N.B. Reis contributed to the original draft preparation, with subsequent review and editing conducted by both authors. All authors have reviewed and approved the final version of the manuscript for publication.

Acknowledgments

This research was sponsored by national funds through FCT-Fundação para a Ciência e a Tecnologia, under the projects UIDB/00285/2020 and LA/P/0112/2020.

Conflict of Interest

The authors declared no potential conflicts of interest concerning the research, authorship, and publication of this article.

Funding

The authors received no financial support for the research, authorship, and publication of this article.

Data Availability Statements

The datasets generated and/or analyzed during the current study are available from the corresponding author on reasonable request.

References

- [1] Hsu, C.F., Tsai, H.Y., Chen, T.H., The Effect of Manufacturing Parameters and Environmental Factors on Mechanical Properties of Carbon Fiber/Epoxy Composites, *Journal of Mechanics*, 34, 2018, 839–846. <https://doi.org/10.1017/jmech.2018.9>.
- [2] Altin Karatas, M., Gökkaya, H., A review on machinability of carbon fiber reinforced polymer (CFRP) and glass fiber reinforced polymer (GFRP) composite materials, *Defence Technology*, 14, 2018, 318–326. <https://doi.org/10.1016/j.dt.2018.02.001>.
- [3] Fakirov, S., Composite materials – is the use of proper definitions important?, *Materials Today*, 18, 2015, 528–529. <https://doi.org/10.1016/j.mattod.2015.10.001>.
- [4] Reis, P.N.B., Ferreira, J.A.M., Zhang, Z.Y., Benameur, T., Richardson, M.O.W., Impact strength of composites with nano-enhanced resin after fire





- exposure, *Composites Part B: Engineering*, 56, 2014, 290–295. <https://doi.org/10.1016/j.compositesb.2013.08.048>.
- [5] Adams, R.D., Cawley, P., A review of defect types and nondestructive testing techniques for composites and bonded joints, *NDT International*, 21, 1988, 208–222. [https://doi.org/10.1016/0308-9126\(88\)90333-1](https://doi.org/10.1016/0308-9126(88)90333-1).
- [6] Amaro, A.M., Reis, P.N.B., De Moura, M.F.S.F., Santos, J.B., Damage detection on laminated composite materials using several NDT techniques, *Insight*, 54, 2012, 14–20. <https://doi.org/10.1784/insi.2012.54.1.14>.
- [7] Reis, P.N.B., Ferreira, J.A.M., Antunes, F.V., Richardson, M.O.W., Effect of Interlayer Delamination on Mechanical Behavior of Carbon/Epoxy Laminates, *Journal of Composite Materials*, 43, 2009, 2609–2621. <https://doi.org/10.1177/0021998309344649>.
- [8] Mosallam, A., Slenk, J., Kreiner, J., Assessment of Residual Tensile Strength of Carbon/Epoxy Composites Subjected to Low-Energy Impact, *Journal of Aerospace Engineering*, 21, 2008, 249–258. [https://doi.org/10.1061/\(ASCE\)0893-1321\(2008\)21:4\(249\)](https://doi.org/10.1061/(ASCE)0893-1321(2008)21:4(249)).
- [9] Mittelman, A., Roman, I., Tensile properties of real unidirectional Kevlar/epoxy composites, *Composites*, 21, 1990, 63–69. [https://doi.org/10.1016/0010-4361\(90\)90099-1](https://doi.org/10.1016/0010-4361(90)90099-1).
- [10] O'Brien, T., Rigamonti, M., Zanotti, C., Tension fatigue analysis and life prediction for composite laminates, *International Journal of Fatigue*, 11, 1989, 379–393. [https://doi.org/10.1016/0142-1123\(89\)90177-1](https://doi.org/10.1016/0142-1123(89)90177-1).
- [11] Amaro, A.M., Reis, P.N.B., De Moura, M.F.S.F., Residual Strength after Low Velocity Impact in Carbon-Epoxy Laminates, *Materials Science Forum*, 514–516, 2006, 624–628. <https://doi.org/10.4028/www.scientific.net/MSF514-516.624>.
- [12] Amaro, A.M., Reis, P.N.B., De Moura, M.F.S.F., Delamination Effect on Bending Behaviour in Carbon-Epoxy Composites: Bending Behaviour in Carbon-Epoxy Composites, *Strain*, 47, 2011, 203–208. <https://doi.org/10.1111/j.1475-1305.2008.00520.x>.
- [13] Ferreira, L.M., Muñoz-Reja, M., Reis, P.N.B., Impact response of semicylindrical woven composite shells: The effect of stacking sequence, *International Journal of Impact Engineering*, 189, 2024, 104952. <https://doi.org/10.1016/j.ijimpeng.2024.104952>.
- [14] Zheng, S., Sun, C.T., Delamination interaction in laminated structures, *Engineering Fracture Mechanics*, 59, 1998, 225–240. [https://doi.org/10.1016/S0013-7944\(97\)00120-3](https://doi.org/10.1016/S0013-7944(97)00120-3).
- [15] De Moura, M., Marques, A., Prediction of low velocity impact damage in carbon-epoxy laminates, *Composites Part A: Applied Science and Manufacturing*, 33, 2002, 361–368. [https://doi.org/10.1016/S1359-835X\(01\)00119-1](https://doi.org/10.1016/S1359-835X(01)00119-1).
- [16] Suemasu, H., Sasaki, W., Ishikawa, T., Aoki, Y., A numerical study on compressive behavior of composite plates with multiple circular delaminations considering delamination propagation, *Composites Science and Technology*, 68, 2008, 2562–2567. <https://doi.org/10.1016/j.compscitech.2008.05.014>.
- [17] Lee, S.-Y., Park, D.-Y., Buckling analysis of laminated composite plates containing delaminations using the enhanced assumed strain solid element, *International Journal of Solids and Structures*, 44, 2007, 8006–8027. <https://doi.org/10.1016/j.ijsolstr.2007.05.023>.
- [18] Amaro, A.M., Reis, P.N.B., De Moura, M.F.S.F., Neto, M.A., Buckling analysis of laminated composite plates submitted to compression after impact, *Fibers and Polymers*, 15, 2014, 560–565. <https://doi.org/10.1007/s12221-014-0560-x>.
- [19] Amaro, A.M., Reis, P.N.B., Neto, M.A., Cirne, J.M., Residual impact strength of carbon/epoxy laminates after flexural loadings, *Composite Structures*, 146, 2016, 69–74. <https://doi.org/10.1016/j.compstruct.2016.03.006>.
- [20] Sasikumar, A., Costa, J., Trias, D., González, E.V., García-Rodríguez, S.M., Maimí, P., Unsymmetrical stacking sequences as a novel approach to tailor damage resistance under out-of-plane impact loading, *Composites Science and Technology*, 173, 2019, 125–135. <https://doi.org/10.1016/j.compscitech.2019.02.002>.
- [21] Sasikumar, A., Trias, D., Costa, J., Singery, V., Linde, P., Mitigating the weak impact response of thin-ply based thin laminates through an unsymmetrical laminate design incorporating intermediate grade plies, *Composite Structures*, 220, 2019, 93–104. <https://doi.org/10.1016/j.compstruct.2019.03.069>.
- [22] Sasikumar, A., García-Rodríguez, S.M., Arbeláez, J.J., Trias, D., Costa, J., On how unsymmetrical laminate designs with tailored ply clusters affect compression after impact strength compared to symmetric baseline, *Composite Structures*, 238, 2020, 111958. <https://doi.org/10.1016/j.compstruct.2020.111958>.
- [23] Reis, P.N.B., Sousa, P., Ferreira, L.M., Coelho, C.A.C.P., Multi-impact response of semicylindrical composite laminated shells with different thicknesses, *Composite Structures*, 310, 2023, 116771. <https://doi.org/10.1016/j.compstruct.2023.116771>.
- [24] Campos, P., Coelho, C.A., Navalho, F.V.P., Reis, P.N.B., Impact response of laminated cylindrical shells, *Frattura ed Integrità Strutturale*, 13, 2019, 411–418. <https://doi.org/10.3221/IGF-ESIS.48.39>.
- [25] Reis, P.N.B., Coelho, C.A.C.P., Navalho, F.V.P., Impact Response of Composite Sandwich Cylindrical Shells, *Applied Sciences*, 11, 2021, 10958. <https://doi.org/10.3390/app112210958>.
- [26] Ferreira, L., Coelho, C., Reis, P., Impact Response of Semi-Cylindrical Composite Laminate Shells Under Repeated Low-Velocity Impacts, *Advances in Science and Engineering Technology International Conferences (ASET)*, 2022. <https://doi.org/10.1109/ASET53988.2022.9735043>.
- [27] Ferreira, L.M., Coelho, C.A.C.P., Reis, P.N.B., Numerical Simulations of the Low-Velocity Impact Response of Semicylindrical Woven Composite Shells, *Materials*, 16, 2023, 3442. <https://doi.org/10.3390/ma16093442>.
- [28] Ferreira, L.M., Coelho, C.A.C.P., Reis, P.N.B., Effect of Cohesive Properties on Low-Velocity Impact Simulations of Woven Composite Shells, *Applied Sciences*, 13, 2023, 6948. <https://doi.org/10.3390/app13126948>.
- [29] Ferreira, L.M., Coelho, C.A.C.P., Reis, P.N.B., Numerical predictions of intralaminar and interlaminar damage in thin composite shells subjected to impact loads, *Thin-Walled Structures*, 192, 2023, 111148. <https://doi.org/10.1016/j.tws.2023.111148>.
- [30] Dassault Systemes. ABAQUS n.d.
- [31] Johnson, A.F., Pickett, A.K., Rozycki, P., Computational methods for predicting impact damage in composite structures, *Composites Science and Technology*, 61, 2001, 2183–2192. [https://doi.org/10.1016/S0266-3538\(01\)00111-7](https://doi.org/10.1016/S0266-3538(01)00111-7).
- [32] Ladeveze, P., LeDantec, E., Damage modelling of the elementary ply for laminated composites, *Composites Science and Technology*, 43, 1992, 257–267. [https://doi.org/10.1016/0266-3538\(92\)90097-M](https://doi.org/10.1016/0266-3538(92)90097-M).
- [33] Hou, J., Measurement of the properties of woven CFRP T300/914 at different strain rates, *Composites Science and Technology*, 60, 2000, 2829–2834. [https://doi.org/10.1016/S0266-3538\(00\)00151-2](https://doi.org/10.1016/S0266-3538(00)00151-2).
- [34] VUMAT for fabric reinforced composites, Dassault Systèmes, 2008.
- [35] Camanho, P.P., Davila, C.G., de Moura, M.F., Numerical Simulation of Mixed-Mode Progressive Delamination in Composite Materials, *Journal of Composite Materials*, 37, 2003, 1415–1438. <https://doi.org/10.1177/0021998303034505>.
- [36] Turon, A., Dávila, C.G., Camanho, P.P., Costa, J., An engineering solution for mesh size effects in the simulation of delamination using cohesive zone models, *Engineering Fracture Mechanics*, 74, 2007, 1665–1682. <https://doi.org/10.1016/j.engfractmech.2006.08.025>.
- [37] Song, K., Dávila, C.G., Rose, C.A., Guidelines and parameter selection for the simulation of progressive delamination, *Abaqus Users' Conference*, 41, 2008, 1–15.
- [38] Nguyen, K.-H., Ju, H.-W., Truong, V.-H., Kweon, J.-H., Delamination analysis of multi-angle composite curved beams using an out-of-autoclave material, *Composite Structures*, 183, 2018, 320–330. <https://doi.org/10.1016/j.compstruct.2017.03.078>.
- [39] Benzeggagh, M.L., Kenane, M., Measurement of mixed-mode delamination fracture toughness of unidirectional glass/epoxy composites with mixed-mode bending apparatus, *Composites Science and Technology*, 56, 1996, 439–449. [https://doi.org/10.1016/0266-3538\(96\)00005-X](https://doi.org/10.1016/0266-3538(96)00005-X).
- [40] Davies, G., Olsson, R., Impact on composite structures, *The Aeronautical Journal*, 108, 2004, 541–563. <https://doi.org/10.1017/S000192400000385>.
- [41] Campilho, R.D.S.G., Moura, D.C., Gonçalves, D.J.S., Da Silva, J.F.M.G., Banea, M.D., Da Silva, L.F.M., Fracture toughness determination of adhesive and co-cured joints in natural fibre composites, *Composites Part B: Engineering*, 50, 2013, 120–126. <https://doi.org/10.1016/j.compositesb.2013.01.025>.
- [42] Reis, P., Ferreira, J., Zhang, Z., Benameur, T., Richardson, M., Impact response of Kevlar composites with nanoclay enhanced epoxy matrix, *Composites Part B: Engineering*, 46, 2013, 7–14. <https://doi.org/10.1016/j.compositesb.2012.10.028>.
- [43] Reis, P., Santos, P., Ferreira, J., Richardson, M., Impact response of sandwich composites with nano-enhanced epoxy resin, *Journal of Reinforced Plastics and Composites*, 32, 2013, 898–906. <https://doi.org/10.1177/0731684413478993>.
- [44] Reis, P.N.B., Neto, M.A., Amaro, A.M., Multi-impact behaviour of composite laminates under constant and different energy levels, *Composite Structures*, 294, 2022, 115788. <https://doi.org/10.1016/j.compstruct.2022.115788>.
- [45] Schoeppner, G.A., Abrate, S., Delamination threshold loads for low velocity impact on composite laminates, *Composites Part A: Applied Science and Manufacturing*, 31, 2000, 903–915. [https://doi.org/10.1016/S1359-835X\(00\)00061-0](https://doi.org/10.1016/S1359-835X(00)00061-0).
- [46] Belingardi, G., Vadori, R., Low velocity impact tests of laminate glass-fiber-epoxy matrix composite material plates, *International Journal of Impact Engineering*, 27, 2002, 213–229. [https://doi.org/10.1016/S0734-743X\(01\)00040-9](https://doi.org/10.1016/S0734-743X(01)00040-9).



- [47] Amaro, A., Reis, P., Neto, M., Louro, C., Effects of alkaline and acid solutions on glass/epoxy composites, *Polymer Degradation and Stability*, 98, 2013, 853–862. <https://doi.org/10.1016/j.polyimdegradstab.2012.12.029>.
- [48] Reis, P., Ferreira, J., Santos, P., Richardson, M., Santos, J., Impact response of Kevlar composites with filled epoxy matrix, *Composite Structures*, 94, 2012, 3520–3528. <https://doi.org/10.1016/j.compstruct.2012.05.025>.
- [49] Amaro, A., Reis, P., Neto, M., Louro, C., Effect of different acid solutions on glass/epoxy composites, *Journal of Reinforced Plastics and Composites*, 32, 2013, 1018–1029. <https://doi.org/10.1177/0731684413483886>.
- [50] Lopes, C.S., Camanho, P.P., Gürdal, Z., Maimí, P., González, E.V., Low-velocity impact damage on dispersed stacking sequence laminates. Part II: Numerical simulations, *Composites Science and Technology*, 69, 2009, 937–947. <https://doi.org/10.1016/j.compscitech.2009.02.015>.
- [51] Abrate, S., *Impact on Composite Structures*, 1st ed. Cambridge University Press, 1998. <https://doi.org/10.1017/CBO9780511574504>.
- [52] Wisnom, M.R., The role of delamination in failure of fibre-reinforced composites, *Philosophical Transactions of the Royal Society A*, 370, 2012, 1850–1870. <https://doi.org/10.1098/rsta.2011.0441>.
- [53] Liv, Y., Guillaumet, G., Costa, J., González, E.V., Marín, L., Mayugo, J.A., Experimental study into compression after impact strength of laminates with conventional and nonconventional ply orientations, *Composites Part B: Engineering*, 126, 2017, 133–142. <https://doi.org/10.1016/j.compositesb.2017.05.074>.
- [54] Sebaey, T.A., González, E.V., Lopes, C.S., Blanco, N., Costa, J., Damage resistance and damage tolerance of dispersed CFRP laminates: Effect of ply clustering, *Composite Structures*, 106, 2013, 96–103. <https://doi.org/10.1016/j.compstruct.2013.05.052>.
- [55] Baker, N., Butler, R., York, C.B., Damage tolerance of fully orthotropic laminates in compression, *Composites Science and Technology*, 2, 2012, 1083–1089. <https://doi.org/10.1016/j.compscitech.2011.09.010>.

ORCID iD

L.M. Ferreira  <https://orcid.org/0000-0002-5223-5309>

C.A.C.P. Coelho  <https://orcid.org/0000-0002-4433-2002>

P.N.B. Reis  <https://orcid.org/0000-0001-5203-3670>



© 2024 Shahid Chamran University of Ahvaz, Ahvaz, Iran. This article is an open access article distributed under the terms and conditions of the Creative Commons Attribution-NonCommercial 4.0 International (CC BY-NC 4.0 license) (<http://creativecommons.org/licenses/by-nc/4.0/>).

How to cite this article: Ferreira L.M., Coelho C.A.C.P., Reis P.N.B. Characterization of Low-Velocity Impact Damage in Asymmetric Composite Shells, *J. Appl. Comput. Mech.*, xx(x), 2024, 1–12. <https://doi.org/10.22055/jacm.2024.45986.4446>

Publisher's Note Shahid Chamran University of Ahvaz remains neutral with regard to jurisdictional claims in published maps and institutional affiliations.

